Journal Pre-proof

Elucidating the microstructural development of refractory metal high entropy superalloys via the Ti–Ta–Zr constituent system

T.E. Whitfield, E.J. Pickering, K.A. Christofidou, C.N. Jones, H.J. Stone, N.G. Jones

PII: S0925-8388(19)34181-7

DOI: https://doi.org/10.1016/j.jallcom.2019.152935

Reference: JALCOM 152935

To appear in: *Journal of Alloys and Compounds*

Received Date: 2 August 2019

Revised Date: 21 October 2019

Accepted Date: 5 November 2019

Please cite this article as: T.E. Whitfield, E.J. Pickering, K.A. Christofidou, C.N. Jones, H.J. Stone, N.G. Jones, Elucidating the microstructural development of refractory metal high entropy superalloys via the Ti–Ta–Zr constituent system, *Journal of Alloys and Compounds* (2019), doi: https://doi.org/10.1016/j.jallcom.2019.152935.

Elucidating the microstructural development of Refractory Metal High Entropy Superalloys via the Ti-Ta-Zr constituent system

T. E. Whitfield[a], E. J. Pickering[b], K. A. Christofidou[a,c], C. N. Jones[d], H. J. Stone[a], N. G. Jones[a*]

a. Department of Materials Science and Metallurgy, University of Cambridge, UK

b. Department of Materials, University of Manchester, UK

c. Department of Materials Science and Engineering, The University of Sheffield, UK

d. Rolls-Royce plc, Derby, UK

* ngj22@cam.ac.uk; 00441223334367

Key words: High Entropy Alloys, high-temperature alloys, microstructure, phase transitions, thermodynamic properties,

Abstract

The recently developed Refractory Metal High Entropy Superalloys have the potential to replace Ni-based alloys in very high temperature structural applications. However, the microstructures of these new alloys typically consist of refractory metal based solid solution precipitates within an ordered superlattice structured matrix, which is likely to compromise key properties such as toughness. As such, there is significant interest in inverting this arrangement, such that superlattice precipitates form within a disordered refractory metal matrix. Yet the mechanisms by which these microstructures form and how they might be modified with compositional variations are currently unclear. To elucidate these mechanisms, the microstructural evolution of a series of compositionally simpler alloys from the Ti-Ta-Zr system have been studied following long term exposures at 700, 900 and 1000˚C. Exposures of up to 1000 hours were used as a proxy to equilibrium and the resulting microstructures were analysed using advanced scanning and transmission electron microscopy methods. The microstructures of these alloys were found to predominantly contain one or two bcc phases, the lengthscale and morphology of which changed with exposure temperature. From these results it is established that the fine-scale microstructure, which is very similar to that widely reported in the more compositionally complex refractory metal high entropy superalloys, forms via spinodal decomposition during cooling. It is also shown, for the first time, how compositional modification can lead to a refractory metal solid solution based matrix. It is believed that these results provide key insights that can guide further development in the more complex systems that will be required for commercial applications.

1. Introduction

Unlike most conventional engineering alloys, High Entropy Alloys (HEAs) consist of multiple principal elements in near-equiatomic concentrations. It has been suggested that the multi-component nature of these alloys would lead to increased stability of solid solution phases due to their high configurational entropies [1-3]. Such extended solubility may help to minimise the formation of deleterious intermetallic phases, enhance properties such as

ductility and toughness, and enable a greater concentration of protective oxide scale forming elements, such as Al, to be present in a solid solution phase [1,3,4]. The compositional space associated with this novel approach is vast and, therefore, requires judicious exploration, but associated with this is the potential to discover and develop new alloy systems that could address demanding engineering problems. One such example would be new materials for use in high temperature structural applications, which require a challenging combination of properties including good mechanical performance and environmental resistance over a wide range of temperatures.

Within the aerospace industry, the requirement to develop more efficient propulsion with lower emissions is leading to hotter, faster rotating cores in the latest gas turbine engines. These changes increase the severity of the inimical conditions experienced by key components. However, the current state-of-the-art materials, nickel-based superalloys, are approaching the physical limits of their development, as operational temperatures are increasing towards their melting points and the densities of these alloys are relatively high [5]. As such, new material solutions must be found if the next generation of gas turbine engines are to be realised.

A recently developed concept that shows promise in this area is that of refractory metal based HEAs (RMHEAs) [3]. Initial research, based on the W-Nb-Mo-Ta-V system, produced single solid solution phase materials that exhibited superior high temperature capability than comparable non-heat treatable commercial nickel-based superalloys [6]. However, the low temperature yield strength of these alloys was significantly inferior than dual phase nickel-based superalloys, such as Inconel 718. In addition, the densities of these early RMHEAs were greater than nickel-based superalloys and no protective scale forming elements were incorporated. As such, more recent attention shifted to extending the RMHEA design concept from single phase solid solutions towards multiphase microstructures, so that precipitation strengthening could be exploited. In particular, there was a desire to incorporate an ordered superlattice phase so as to emulate the ɣ -ɣ’ microstructure, which helps to confer the excellent high temperature mechanical properties of nickel based superalloys.

The multi-phase Refractory Metal High Entropy Superalloys (RMHES) developed, such as $AlMo_{0.5}NbTa_{0.5}TiZr$, show greater high temperature compressive strengths and a lower density than several commonly used polycrystalline nickel-based superalloys [7,8]. This multi-phase alloy, and closely related compositional variants, has a fine-scale intragranular microstructure, consisting of cuboidal and plate-like particles of an A2 (Strukturbericht notation corresponding to the bcc structure) phase in an ordered B2 superlattice matrix [9]. Grain boundary precipitates of an Al and Zr rich intermetallic have also been reported [7,10]. However, this microstructure, comprising solid solution precipitates in an intermetallic matrix, is the inverse of those found in nickel-based superalloys. Critically, the presence of an ordered B2 matrix is thought to hinder the ductility of these alloys due to the limited plastic flow typically exhibited by ordered phases. Consequently, there is significant interest in establishing a methodology by which the microstructure can be inverted.

Attempts to achieve an inverted microstructure through compositional variations in this system have not been successful to date [10]. Nevertheless, it has been reported that

ordered B2 precipitates can be formed within the bcc matrix of $Al_{0.5}NbTa_{0.8}Ti_{1.5}V_{0.2}Zr$ when subjected to a specific series of heat treatments [11,12]. However, the exact mechanisms by which this inversion occurs are not yet fully understood. As such, further work is required to understand the microstructural evolution in multi-phase RMHES to establish whether compositional modifications are able to achieve the desired combination of phases.

At present, there is limited information available on to the thermodynamic and kinetic factors contributing to the formation of the two phase microstructure. Although, it has been suggested that it may be a result of a spinodal decomposition [5,12]. Detailed analysis of the fine two phase microstructure of $AlMo_{0.5}NbTa_{0.5}TiZr$ [5,9] has shown the B2 matrix phase to be rich in Al and Zr, whilst the bcc regions were richer in the refractory components Nb, Mo, and Ta. The Ti content of the alloys showed a slight preference for the Zr and Al-rich phase although its partitioning between the two phases was very similar. Consequently, it has been proposed that the two phase formation in $AlMo_{0.5}NbTa_{0.5}TiZr$ is driven by the miscibility gap in either the Ta-Zr or Nb-Zr systems [10]. However, it should be noted that a spinodal decomposition would not produce the B2 phase from the parent bcc phase and, therefore, an additional ordering transformation must also occur in $AlMo_{0.5}NbTa_{0.5}TiZr$.

Theoretically, it should be possible to invert a microstructure formed through a spinodal decomposition by varying the alloy composition such that the parent phase lies on the opposite side of the Gibbs energy maxima associated with the miscibility gap [13]. However, the compositional complexity of these alloys makes it difficult to study the effects of the different alloying elements and it is also not known which constituents play the key roles in developing the microstructural features observed. Therefore, one approach to gaining a better understanding of how the microstructure of these alloys develop is through the characterisation of key compositionally simpler constituent systems. In the case of $AlMo_{0.5}NbTa_{0.5}TiZr$ and related alloys, a perceived key system is the Ti-Ta-Zr ternary, as both Ta and Zr are completely soluble in binary alloys with Ti at elevated temperatures, whilst a large miscibility gap exists in the Ta – Zr binary phase diagram [5,9]. However, little is known about the behaviour of the corresponding ternary system and the phase diagrams that exist have been computationally produced by extrapolation from experimental binary alloy data [14]. As such, an experimental investigation of the ternary system is crucial for understanding the influence of composition on the microstructures formed in this system. To meet this need, this manuscript reports on an investigation of the phase equilibria and microstructural formation sequences of a systematic series of Ti-Ta-Zr alloys following long duration exposures at temperatures of 700, 900 and 1000˚C. Given that Al is thought to drive the ordering reaction that leads to formation of the B2 phase in $AlMo_{0.5}NbTa_{0.5}TiZr$ [10], its absence in this simplified system is likely to result in only disordered phases.

2. Methods

To study the phase equilibria of the Ti-Ta-Zr system a series of alloys with a fixed Ti content and varying concentrations of Ta and Zr were produced via arc melting from elemental metals (≥ 99.5 % purity). The nominal compositions of these alloys were: 45Ti-15Ta-40Zr, 45Ti-25Ta-30Zr, 45Ti-35Ta-20Zr and 45Ti-45Ta-10Zr at.%, as shown in Figure 1. From here on in, these compositions will be referred to as Alloy 1540, Alloy 2530, Alloy 3520 and Alloy 4510 respectively. Each alloy was fabricated under an inert Ar atmosphere, which had also been gettered by melting an ingot of pure Ti prior to the alloy. To enhance macroscopic homogeneity, each ingot was inverted and re-melted a total of eight times. Following melting, the ingots were solution heat treated at 1200 ˚C for 100 hours and quenched into iced water. Further heat treatments were conducted for 1000 hours on 10 mm transverse sections at temperatures of 700, 900 and 1000 ˚C followed by ice water quenching. In all cases, heat treatments were carried out with samples wrapped in a Ta foil getter and sealed in quartz tubes under vacuum.

The actual compositions of the alloys were determined from solution heat treated material at an external laboratory using certified X-ray Fluorescence Spectroscopy (XRF) and fusion – thermal conductivity methodologies.

Material from each stage of the process was prepared for scanning electron microscopy (SEM) analysis by grinding with successively finer grades of SiC paper before final polishing with a buffered colloidal silica solution to provide a 0.06 µm finish. The samples were analysed using back scattered electron (BSE) imaging on an FEI Nova NanoSEM 450 SEM, and a Zeiss GeminiSEM 300. Elemental distribution maps were obtained via an Oxford Instruments X-Max^N 50 energy dispersive X-ray (EDX) detector in the Zeiss SEM.

In order to image the fine-scale features within the microstructures, higher resolution analysis was conducted using Transmission Electron Microscopy (TEM). Electron transparent samples were prepared using an FEI Helios dual-beam focused ion beam (FIB) instrument and were investigated in an FEI Talos F200X Scanning Transmission Electron Microscope (STEM), equipped with Super EDX detectors and operated at 200kV.

3. Results

Microstructural examination of the as-cast alloys using BSE imaging and EDX analysis showed dendritic microsegregation with Ta rich dendrites and Zr rich interdendritic regions. EDX mapping showed that a solution heat treatment of 100 hours at 1200˚C was sufficient to homogenise the alloys and eliminate the prior dendritic segregation, achieving an even distribution of the constituent elements, to the resolution limits of the instrument. As an example of this process, data corresponding to Alloy 4510, which has the greatest refractory metal content, is shown in Figure 2.

The measured compositions of the experimental alloys, performed on solution heat treated material from each of the alloys using certified methodologies, are shown in Table 1. The elemental concentrations in each alloy were within 1.2 at.% of the intended values, with the exception of Alloy 4510, where there was a slight increase in the concentration of Ta with respect to Ti. Nevertheless, this variation was not believed to unduly compromise the systematic nature of this alloy series.

Table 1: Measured alloy compositions, determined by XRF and fusion – thermal conductivity.

Alloy	Alloy designation	Ti (at.%)	Ta (at.%)	Zr (at.%)	O (wt ppm)
Ti-15Ta-40Zr	1540	45.2	14.8	40.0	732
Ti-25Ta-30Zr	2530	45.2	24.5	30.3	401
Ti-35Ta-20Zr	3520	43.8	36.1	20.1	309
Ti-45Ta-10Zr	4510	42.3	48.2	9.5	484

Backscattered electron images of each alloy following solution heat treatment at 1200˚C are presented in Figure 3. At high magnification very fine basketweave type microstructures were seen in Alloys 1540, 2530 and 3520, with a length scale estimated to be in the range of 10-25 nm. No fine microstructural features could be seen in Alloy 4510, which contained the highest concentration of Ta. These observations suggest that at 1200˚C all of the alloys are within a single phase field and that the evolution of the fine-scale microstructures observed in Alloys 1540, 2530 and 3520 were likely to have occurred during cooling.

The microstructures of the alloys following 1000-hour heat treatments at 1000, 900 and 700˚C can be seen in Figure 4 (lower magnification) and Figure 5 (higher magnification). Following exposure at 1000˚C, no evidence of any coarse particles was observed within the microstructure of any of the alloys, Figure 4. Higher magnification imaging, Figure 5, revealed a fine-scale basketweave structure, similar to that observed in the solution heat treated condition, in all of the samples except that of Alloy 4510. This would suggest that all of the alloys are still within a single phase field, which persists across a wide swathe of compositional space to temperatures of at least 1000˚C .

Following exposure at 900˚C, the microstructure of Alloys 1540 and 4510 continued to be devoid of any larger scale features, Figure 4. Fine-scale particles, akin to those seen in both the solution heat treated condition and material exposed at 1000˚C, were observed within the microstructure of Alloy 1540, whilst Alloy 4510 remained featureless. In contrast, the microstructures of Alloys 2530 and 3520 contained relatively coarse particles, which had a brighter BSE contrast than the surrounding matrix. A marked difference in the volume fraction of these particles was observed between the two alloys, with Alloy 3520 having a significantly greater fraction of the bright contrast phase than Alloy 2530. The elemental partitioning between these particles and the surrounding matrix was assessed via SEM based EDX mapping, with an example from Alloy 2530 shown in Figure 6. The grey matrix phase was clearly enriched in Zr, whilst the bright particles predominantly consisted of Ta. The partitioning of Ti between these two phases was less pronounced, with both phases containing a significant concentration of this element, albeit in slightly greater concentrations in the Zr-rich matrix. Quantitative analysis of the EDX signal obtained from these two phases indicated that the matrix had a composition of approximately Ti-21Ta-33Zr (at.%), whilst the bright particles had a composition of approximately Ti-52Ta-11Zr (at.%). In between these coarse particles a very fine-scale basketweave structure, akin to that seen in Alloy 1540, was observed, Figure 5.

Long duration exposure at 700˚C led to the formation of coarse particles in all of the studied alloys, albeit at different length scales. Alloys 1540 and 2530 exhibited round bright contrast particles, with diameters on the order of 5 – 15 μm, within a darker contrast matrix. These features were consistent with the observations for Alloys 2530 and 3520 following exposure at 900˚C. The particles were observed to have formed both intragranularly and along the grain boundaries for Alloys 1540 and 2530. Alloy 3520 exhibited similar microstructural features, however, the coarse particles were only observed along the grain boundaries. Within the grains, Alloys 2530 and 3520 also contained bright particles, on the 100 nm scale, which had a more blocky morphology than the larger spherical particles, shown in Figure 4. Within the Ti and Zr-rich phase additional nanometer scale features could be observed, Figure 5. Alloy 1540 exhibited a basketweave structure within the darker contrast matrix, similar to that seen following higher temperature exposures. A markedly different fine-scale structure was seen in Alloys 2530 and 3520. Within the Ti and Zr-rich phase, dark laths, which were significantly larger than the length scale of the basketweave structure previously observed, were found. In between these laths, small regions of bright BSE contrast, ~5-15 nm, were observed suggesting a local enrichment of Ta.

Unlike all of the other conditions described thus far, the microstructure of Alloy 4510 following exposure at 700˚C exhibited a bright contrast matrix within which darker contrast particles were observed. These particles were several hundred nanometres in size and had a blocky morphology, similar to the blocky features seen in Alloys 2530 and 3520. Within these dark particles there was evidence of further fine-scale features, including darker contrast laths and potentially a basketweave structure.

To study the crystallographic nature and elemental partitioning of these fine-scale phases in more detail, TEM based techniques were used. An example of these data, acquired from Alloy 2530 following a 1000-hour exposure at 1000˚C, are shown in Figure 7. The

basketweave structure was found to comprise alternating regions of compositionally distinct phases, one enriched in Ta and the other in Ti and Zr. In addition, the Ta rich phase was also observed to delineate the grain boundaries. A selected area electron diffraction pattern (SADP) acquired along a $<110>_{bcc}$ zone axis from within the grain marked A is also included in Figure 7. The SADP contained strong reflections corresponding to the bcc structure, as well as diffracted intensity at ~ 1/3 and 2/3 $<112>_{bcc}$, indicative of the omega phase commonly found in metastable beta Ti alloys [15-19]. This would suggest that both the Ta-rich and the Ti and Zr-rich phases had a bcc structure and that one of these, probably the Ti and Zr-rich phase, contained the omega phase.

Within the SADP shown in Figure 7, regions of faint intensity could be observed at ½ $<112>_{bcc}$, which might indicate the presence of an orthorhombic phase. However, line profile analysis along this direction indicated that the intensities of these spots were lower than those of the neighbouring omega reflections and, given the visible reciprocal lattice streaking along the $<112>_{bcc}$, it is also possible that this signal could result from the intersection of diffuse scattering. As such, the presence of intensity at ½ $<112>_{bcc}$ was not taken as conclusive evidence of the presence of an additional phase in this material condition.

In contrast to Alloys 1540, 2530 and 3520, no fine-scale features could be observed within the microstructure of Alloy 4510 following the 1000-hour exposure at 1000˚C, Figure 5. The TEM-based studies performed on this material are shown in Figure 8. An SADP acquired from region A of this material along a $<110>_{bcc}$ zone axis contained strong bcc reflections and additional diffuse reciprocal lattice streaking along the $<112>_{bcc}$ directions. Such streaking has been associated with the presence of diffuse or incommensurate omega structures in metastable beta titanium alloys, although its presence is not necessarily conclusive [20,21].

TEM-based data obtained following 1000 h at 700˚C were acquired from Alloys 2530, 3520 and 4510. The results corresponding to Alloys 3520 and 4510 are shown in Figure 9 and Figure 10 respectively. The microstructures of Alloys 2530 (see supplementary data for corresponding TEM results) and 3520 were very similar, with the exception of the difference in phase fractions evident in corresponding SEM images shown in Figure 5. As can be seen in Figure 9, these microstructures contained two major phases. The bright contrast features in the high angle annular dark field (HAADF) image were enriched in Ta, whilst the dark contrast features were enriched in Ti & Zr. SADPs from the two phases indicated that they both had a bcc structure and, given that both patterns shown in Figure 9 were acquired from a single tilt condition, these structures were similarly oriented. Whilst the diffraction pattern from the bright contrast Ta rich phase, SADP B in Figure 9, contained reflections corresponding to a bcc structure only, the diffraction pattern obtained from the Ti- and Zr-rich phase, SADP A in Figure 9, contained multiple additional reflections as well as those relating to a bcc structure. Specifically, pronounced points of intensity were observed at 1/3 and 2/3 $<112>_{bcc}$, consistent with the omega phase, as well as distinct spots present at ½ $<112>_{bcc}$, which, as mentioned above, could indicate the presence of an orthorhombic phase. The relationship between these reflections and the corresponding crystal structures are shown in the key diagram, where reflections attributed to double diffraction are also indicated.

A number of potential nanoscale orthorhombic phases have been reported in metastable β titanium alloys, including α″ martensite, O′ and O″ [21-27] . The diffraction patterns corresponding to the O″ phase would include two additional reflections between (XX0) reflections, which are not observed in the present study [26]. A dark field image formed from the three non-bcc reflections that lie on the $<112>_{bcc}$ is shown in Figure 11. This image highlights elongated lath-like features within the microstructure, which are on the order of 100 – 200 nm in length. Such morphology and size would seem to be more consistent with that of the α″ martensite rather than the nanodomains reported for the O′ phase [25,27].

The microstructure of Alloy 4510 was markedly different to those of Alloys 2530 and 3520 following 1000 hour exposure at 700˚C. The HAADF image of this material, Figure 10, showed a continuous bright contrast matrix that was found to be Ta-rich from the STEM EDX data. The dark contrast regions within this matrix correspond to the Ti- and Zr-rich phase. Therefore, this alloy exhibits an inverted microstructure to that of Alloys 2530 and 3520. SADPs were acquired from both phases at a single tilt condition, which again indicated that both phases had very similar crystallographic orientations. As with the data presented for Alloys 2530 and 3520, the SADPs acquired from the Ta rich phase in Alloy 4510, SADP B in Figure 10, showed reflections that were solely related to a bcc structure, with no evidence of any other signal. However, whilst the SADP from the Ti- and Zr-rich phase also indicated the presence of a similarly orientated bcc structure, these regions also contained pronounced diffracted intensity at 1/3 and 2/3 $<112>_{bcc}$, suggesting the presence of the omega phase.

4. Discussion

The microstructure of all of the alloys studied were either single phase or contained only the fine-scale basketweave structures following exposure at 1000˚C or above. The length scales of the features observed were too fine to have evolved during this prolonged thermal treatment and, thus, are thought to have formed on cooling. Consequently, it is believed that at temperatures above 1000˚C there is complete miscibility along the studied composition line and all of these alloys are in a single phase condition.

The basketweave structures are similar to those reported in the more complex refractory metal HEAs, e.g. $AlMo_{0.5}NbTa_{0.5}TiZr$. They consist of two phases with cubes and plates of a Ta rich phase, on the order of 20nm, within a Ti and Zr rich matrix. These observations indicate that compositional complexity alone is not required to drive the formation of microstructures with this morphology in RMHES. It is recognised that the phases observed in the present work do not correspond directly to those in the RMHES, as the ordered B2 phase was not present. However, as highlighted in the introduction, this was expected as a result of the deliberate exclusion of Al and, in fact, demonstrates that the ordering caused by the Al is not required to create the fine-scale microstructure.

The formation of Ta and Zr enriched phases at 700˚C in all of the alloys and in Alloy 2530 and 3520 at 900˚C corresponds well with the predicted miscibility gap between Ta and Zr shown in the phase diagram of the Ti-Ta-Zr system in Figure 1. As such, the driving force for the microstructures obtained in Alloys 1540, 2530 and 3520, which are similar to those reported in $AlMo_{0.5}NbTa_{0.5}TiZr$, must be a result of the Ta-Zr miscibility gap. Consequently,

these results suggest that the Ta-Zr miscibility gap could be responsible for the phase formation observed in $AlMo_{0.5}NbTa_{0.5}TiZr$, although similar miscibility gaps in other RM systems may also contribute.

From the data presented, it is clear that the larger precipitates and the fine-scale basketweave structures formed by different mechanisms. The larger precipitates formed when the material was heat treated in a two phase region, most likely through classical nucleation and growth processes. Since, both of these phases have bcc crystal structures, the corresponding Gibbs energy curve must contain two distinct minima, as shown by the large two phase field within the calculated phase diagram shown in Figure 1. However, the fine-scale basketweave structures form during rapid cooling, where there is insufficient time for long range diffusional processes to occur. Nevertheless, clear compositional differences were observed between the two phases that appeared to be similar to those of the larger precipitates formed during heat treatment. These observations collectively suggest that these fine-scale features form through a spinodal decomposition, consistent with the microstructural formation mechanism proposed for the more compositionally complex RMHES [5,12].

The occurrence of the fine-scale basketweave structure in the microstructures of Alloys 2530 and 3520 following exposure at 900˚C and in Alloy 1540 and 4510 following exposure at 700˚C, where the material is already in a two phase region is interesting. The basketweave structure was only observed within the Ti and Zr based phase, whilst the Ta-rich phase showed no evidence of decomposition. These observations suggest that the composition of the Ti- and Zr- rich phase at elevated temperatures lies within the spinodal region of the Ta and Zr miscibility gap at lower temperatures, thereby leading to splitting into compositionally distinct phases on cooling. In contrast, the composition of the Ta-rich phase lies outside the spinodal region and, therefore, does not undergo further decomposition when rapidly cooled. This situation would require the miscibility gap in the Ti-Ta-Zr system to be asymmetric, which is entirely plausible in multi-dimensional composition space.

Following exposure at 700˚C, the Ti- and Zr-rich phase in Alloy 2530 and Alloy 3520 did not show the basketweave structure but instead contained larger nanoscale laths and very fine Ta-rich particles. The SADPs from these regions, contained evidence of an orthorhombic phase, which could be the α" martensite found in metastable beta titanium alloys [21-24]. Given the high concentration of Ti and Zr in this phase and the lower concentration of Ta, which is a beta phase stabilising element, it would not be surprising if the martensite phase were to form during rapid cooling. The prevalence of the martensite following exposure at 700˚C is believed to be related to the lengthscale of the microstructure. During the thermal exposure, the driving force for nucleation of the Ta-rich precipitates will be lower at 900˚C than at 700˚C. As such, the average interparticle spacing between Ta-rich precipitates will be greater at 900˚C. Therefore, it is possible that, despite the enhanced kinetics at 900˚C, the distance between these particles may be greater than the elemental diffusional distances in this alloy. Consequently, compositional gradients might exist around the Ta-rich precipitates leading to a region that does not form the basketweave structure when rapidly cooled. Clear evidence of such a zone is shown in Figure 5. At lower temperatures, for example 700˚C, the interparticle spacing is smaller due to the greater driving force for

nucleation and it is conceivable that this separation is of similar magnitude to the elemental diffusional distances. Therefore, no large compositional gradients would be expected and, given the greater extent of elemental partitioning between the phases, the Ti- and Zr-rich phase becomes susceptible to a martensitic transformation, as seen in Figure 5. Further evidence for this hypothesis can be seen in Figure 12, which shows the microstructure of Alloy 3520 following rapid cooling from the 900˚C in more detail. Within the basketweave free regions surrounding the Ta precipitates darker BSE contrast laths are visible, similar to those observed in the samples exposed at 700˚C, which would be consistent with the diffusion based compositional gradient theory proposed above.

Around the martensitic laths, bright BSE contrast particles were present, Figure 5, which implies that a spinodal decomposition can also occur in this phase. Such features are not commonly observed in metastable beta titanium alloys and could suggest that local compositional fluctuations exist within the Ti- and Zr-rich phase, although verification of this is beyond the scope of the current work and requires further investigation.

Critically, the systematic variation of alloy compositions in the present work has shown that the microstructural evolution is dominated by the miscibility gap between Ta and Zr. In particular, the results indicate that the fine-scale microstructure, similar to that observed in RMHES, is a result of a spinodal decomposition. In addition, it has been shown that with a sufficiently high Ta:Zr ratio the matrix material becomes refractory metal rich and contains Ti- and Zr- rich particles. This partitioning is opposite to that commonly observed in the microstructures of multicomponent RMHES. Within these more complex alloys the Al strongly partitions to the Ti- and Zr- rich phase, causing it to order and adopt the B2 structure. As such, the ability to form a refractory metal solid solution matrix in the constituent Ti-Ta-Zr ternary system, suggests that microstructural inversion may be possible through compositional alterations in Al-containing alloys. However, in the alloy with the highest Ta content (Alloy 4510), spinodal decomposition was not observed to occur in this refractory metal rich matrix phase, potentially indicating a limit to the ability to form the fine-scale two phase microstructures desired. Further exploration, both within this ternary system and through higher order alloying, may resolve this issue but the present study has demonstrated that it is possible to produce a refractory metal based solid solution matrix in these systems through compositional changes.

5. Conclusions

To help elucidate the microstructural evolution of the compositionally complex RMHES, the phase equilibria of a systematic series of alloys within the Ti-Ta-Zr system have been investigated at temperatures of 700, 900 and 1000˚C. From this study, the following conclusions have been drawn:

- At temperatures above 1000˚C a single bcc solid solution phase field was found for all of the alloys considered.

- At lower temperatures a two phase region existed and was found to be in good agreement with previously published phase diagram predictions.

- Following quenching from the single phase field a fine-scale basketweave like structure was obtained, which is extremely similar to those reported in RMHES. This observation suggests that such microstructures are not unique to compositionally complex RMHES and validates the concept of studying compositionally simpler systems.

- The microstructural constituents of these alloys are dominated by the miscibility gap between Ta and Zr and the formation of the fine-scale features shown to be a result of spinodal decomposition.

- The results show that a refractory metal based matrix phase can be obtained in this system by compositional modification, an observation that could be highly significant, as it may aid the development of new RMHES with solid solution, as opposed to ordered, matrices.

- The refractory metal rich matrix phase appeared to be outside of the spinodal region and, therefore, did not form the fine-scale features observed in the other alloys.

Acknowledgements

The authors would like to thank Dr H. T. Pang and S. Rhodes for their experimental assistance. TEW, NGJ and HJS would like to acknowledge the support of the EPSRC/Rolls-Royce Strategic Partnership under EP/M005607/1. FIB liftout of TEM samples was performed by Dr G. West at the WMG, University of Warwick. The authors also acknowledge the support of the Henry Royce Institute for access to the FEI Talos electron microscope at Royce@Manchester (EP/R00661X/1). The underlying research data from this work can be found at www.data.cam.ac.uk.

References

[1] J.W. Yeh, S.K. Chen, S.J. Lin, J.Y. Gan, T.S. Chin, T.T. Shun, C.H. Tsau, S.Y. Chang, Advanced Engineering Materials 6 (2004) 299–303.

[2] B. Cantor, I.T.H. Chang, P. Knight, A.J.B. Vincent, Materials Science & Engineering A 375-377 (2004) 213–218.

[3] D.B. Miracle, O.N. Senkov, Acta Materialia 122 (2017) 448–511.

[4] E.J. Pickering, N.G. Jones, International Materials Reviews 61 (2016) 183–202.

[5] O. Senkov, D. Isheim, D. Seidman, A. Pilchak, Entropy 18 (2016) 102–13.

[6] O.N. Senkov, G.B. Wilks, J.M. Scott, D.B. Miracle, Intermetallics 19 (2011) 698–706.

[7] O.N. Senkov, S.V. Senkova, C. Woodward, Acta Materialia 68 (2014) 214–228.

[8] O.N. Senkov, C. Woodward, D.B. Miracle, JOM 66 (2014) 2030–2042.

[9] J.K. Jensen, B.A. Welk, R.E.A. Williams, J.M. Sosa, D.E. Huber, O.N. Senkov, G.B. Viswanathan, H.L. Fraser, Scripta Materialia 121 (2016) 1–4.

[10] O.N. Senkov, J.K. Jensen, A.L. Pilchak, D.B. Miracle, H.L. Fraser, Materials & Design 139 (2018) 498–511.

[11] V. Soni, O.N. Senkov, B. Gwalani, D.B. Miracle, R. Banerjee, Scientific Reports 8 (2018) 1–10.

[12] V. Soni, B. Gwalani, O.N. Senkov, B. Viswanathan, T. Alam, D.B. Miracle, R. Banerjee, Journal of Materials Research 33 (2018) 3235–3246.

[13] P. Haasen, R. W. Cahn Physical Metallurgy (2004) 1–1042.

[14] L. Lin, L. Delaey, O. Van Der Biest, P. Wollants, Scripta Materialia 34 (1996) 1411–1416.

[15] E.L. Pang, E.J. Pickering, S.I. Baik, D.N. Seidman, N.G. Jones, Acta Materialia 153 (2018) 62–70.

[16] S.L. Sass, Acta Metallurgica 17 (1969) 813–820.

[17] C. Goasdoue, P.S. Ho, S.L. Sass, Acta Metallurgica 20 (1972) 725–733.

[18] S.K. Sikka, Y.K. Vohra, R. Chidambaram, Progress in Materials Science 27 (1982) 245–310.

[19] S.L. Sass, Journal of the Less Common Metals 28 (1972) 157–173.

[20] J.M. Bennett, E.J. Pickering, J.S. Barnard, D. Rugg, H.J. Stone, N.G. Jones, Materials Characterization 142 (2018) 523–530.

[21] E.W. Collings, The Physical Metallurgy of Titanium Alloys, American Society for Metals, 1984.

[22] M. Li, X. Min, K. Yao, F. Ye, Acta Materialia 164 (2019) 322–333.

[23] C.A.F. Salvador, E.S.N. Lopes, C.A. Ospina, R. Caram, Materials Chemistry and Physics 183 (2016) 238–246.

[24] D. Banerjee, J.C. Williams, Acta Materialia 61 (2013) 844–879.

[25] Y. Zheng, D. Banerjee, H.L. Fraser, Scripta Materialia 116 (2016) 131–134.

[26] Y. Zheng, R.E.A. Williams, H.L. Fraser, Scripta Materialia 113 (2016) 202–205.

[27] Y. Zheng, R.E.A. Williams, S. Nag, R. Banerjee, H.L. Fraser, D. Banerjee, Scripta Materialia 116 (2016) 49–52.

Figure 1: Predicted Ti-Ta-Zr phase diagram at 900˚C (adapted from [14]) with the nominal composition of the alloys investigated in this study superimposed.

Figure 2: BSE images and corresponding EDX elemental partitioning maps for Alloy 4510 in the as-cast and solution heat treated conditions.

Figure 3: BSE images of the Alloys 1540, 2530, 3540 and 4510 in the homogenised state.

Figure 4: BSE images of Alloys 1540, 2530, 3520 and 4510 after 1000 hours at 1000, 900 and 700˚C.

Figure 5: Higher magnification BSE images of Alloys 1540, 2530, 3520 and 4510 after 1000 hours at 1000, 900 and 700˚C.

Figure 6: BSE image and corresponding EDX elemental distribution maps for Ti, Ta and Zr from Alloy 2530 after exposure at 900˚C for 1000 hours showing the partitioning of elements between phases.

Figure 7: TEM HAADF image of Alloy 2530 along a grain boundary after exposure at 1000˚C for 1000 hours and corresponding STEM EDX elemental distribution maps for Ti, Ta and Zr. An SADP from grain A and the related key diagram are also shown, indicating the presence of bcc and omega phases.

Figure 8: TEM HAADF image and STEM EDX elemental maps for Ti, Ta and Zr acquired from Alloy 4510 after exposure at 1000˚C for 1000 hours. The corresponding SADP from region A contains bcc reflections and streaks along the $<112>_{bcc}$, as shown in the related key diagram.

Figure 9:HAADF image and STEM EDX elemental distribution maps for Ti, Ta and Zr acquired from Alloy 3520 after exposure for 1000 hours at 700˚C. The SADP from a Ta enriched region (B) showed only bcc reflections whilst the SADP from a Ti and Zr enriched region (A) also contains omega and orthorhombic phase reflections.

Figure 10: HAADF image and STEM EDX elemental distribution maps for Ti, Ta and Zr acquired form Alloy 4510 after exposure to 700˚C for 1000 hours. An SADP from a Ta rich region (B) showed only bcc reflections whilst the SADP from a Ti and Zr enriched region (A) also contains reflections from the omega phase.

Figure 11: Dark field image of Alloy 3520 after exposure at 700˚C for 1000 hours taken using the three non-bcc reflections that lie on the $<112>_{bcc}$ in Figure 9.

Figure 12: Higher magnification BSE image of Alloy 3520 after 1000 hours at 900˚C.

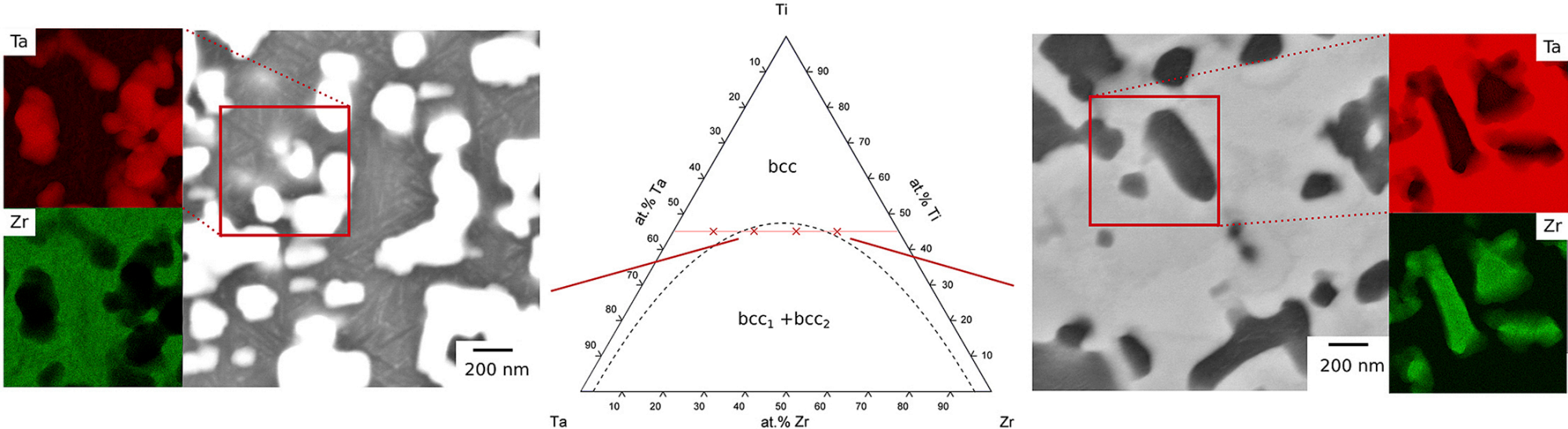
Ta
Zr
200 nm
Ti
bcc
bcc$_1$ +bcc$_2$
at.% Ta
at.% Ti
at.% Zr
Ta
Zr
10
20
30
40
50
60
70
80
90
Ta
Zr
200 nm

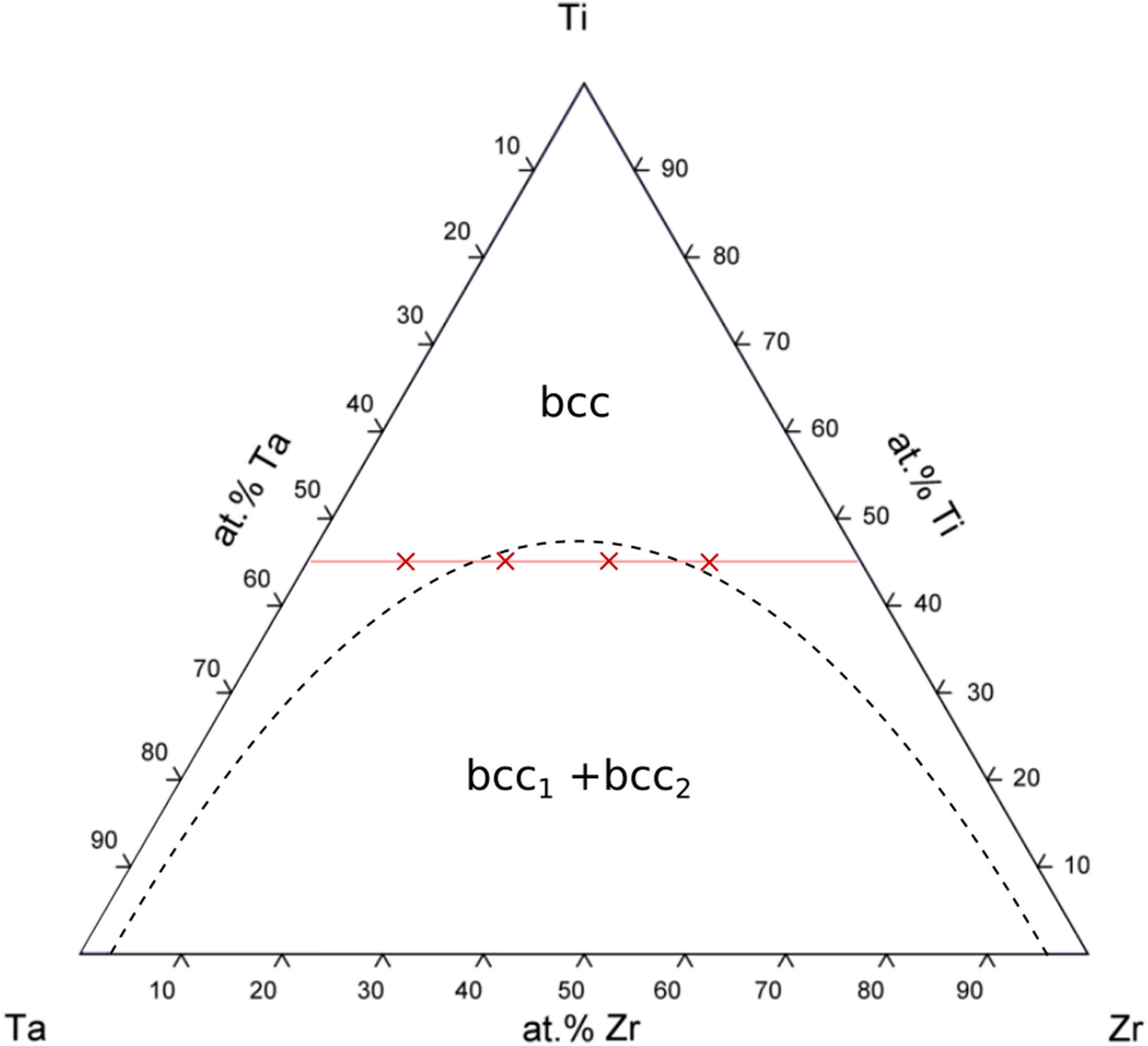
Ti
10
90
20
80
30
70
40
60
50
50
60
40
70
30
80
20
90
10
at.% Ta
at.% Ti
bcc
bcc1 +bcc2
10
20
30
40
50
60
70
80
90
Ta
at.% Zr
Zr

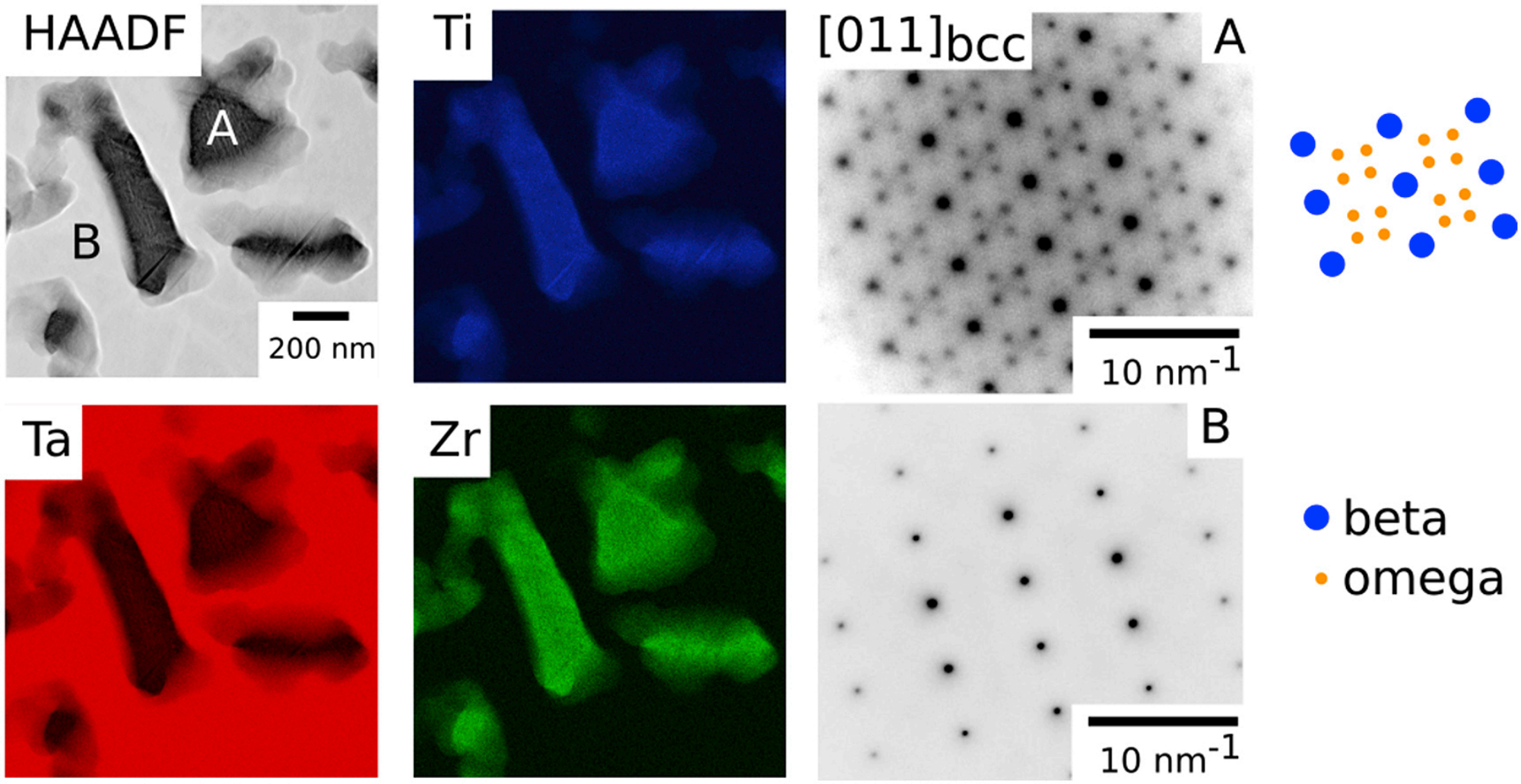
HAADF
A
B
200 nm
Ti
[011]bcc
A
10 nm-1
Ta
Zr
B
10 nm-1
beta
omega

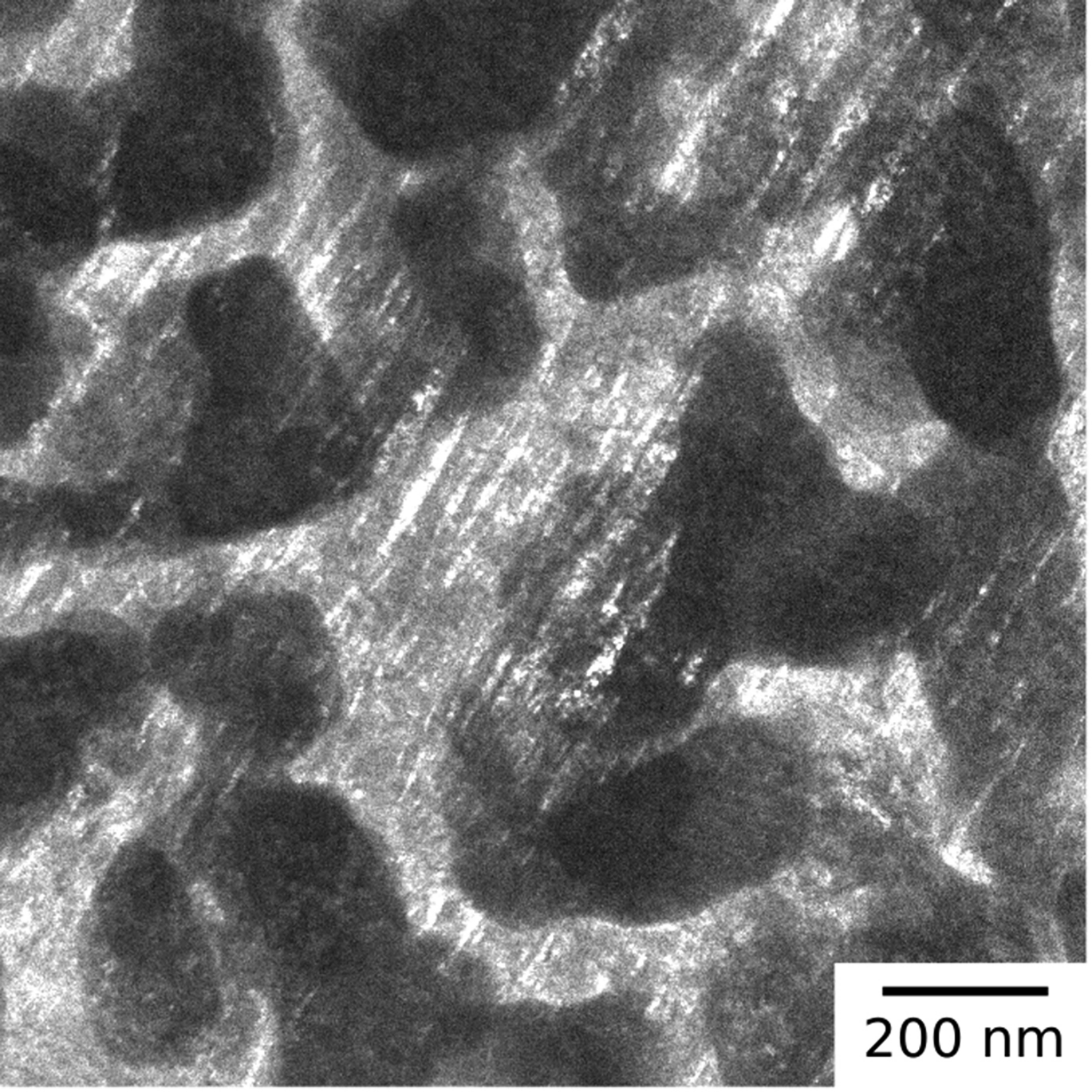
200 nm

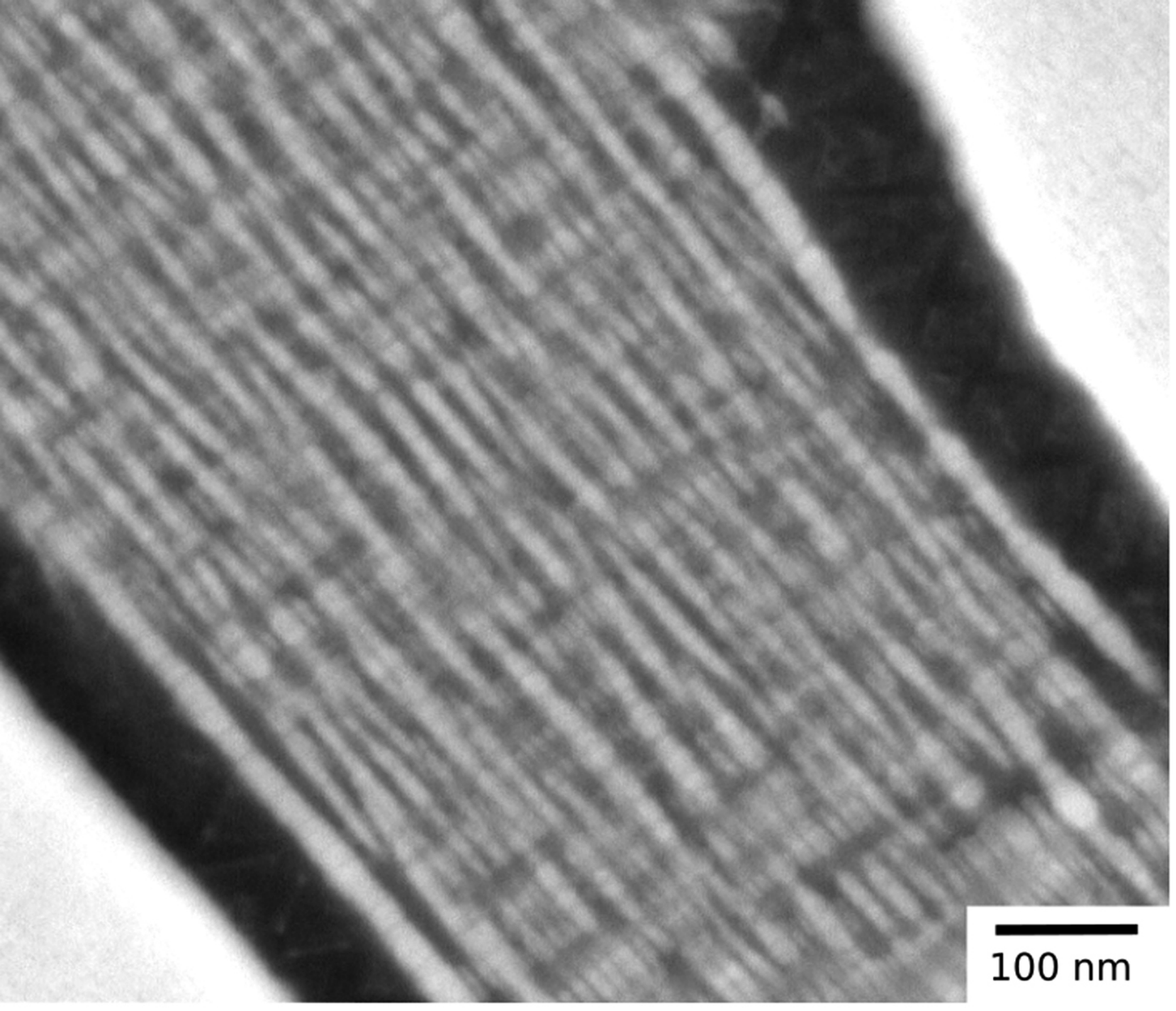
100 nm

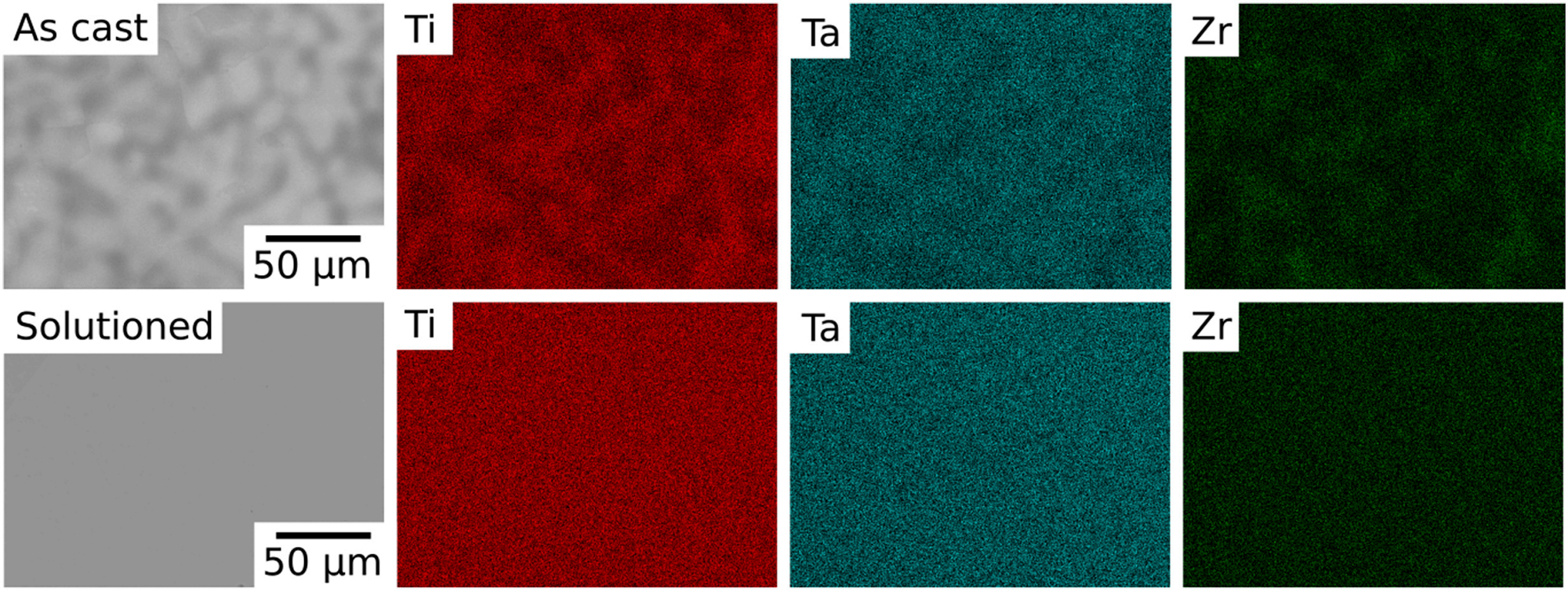
As cast
50 µm
Ti
Ta
Zr
Solutioned
50 µm
Ti
Ta
Zr

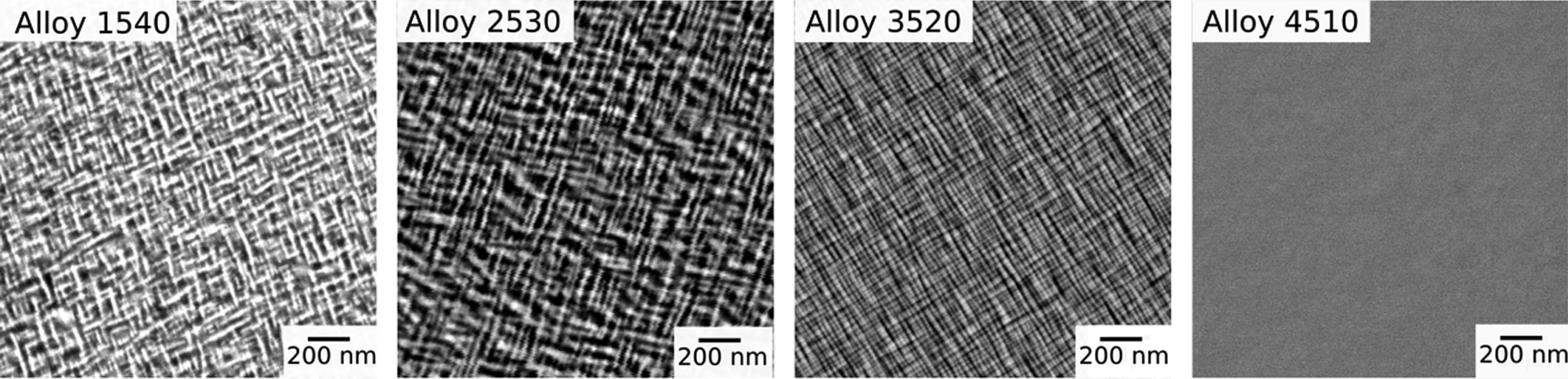
Alloy 1540
200 nm
Alloy 2530
200 nm
Alloy 3520
200 nm
Alloy 4510
200 nm

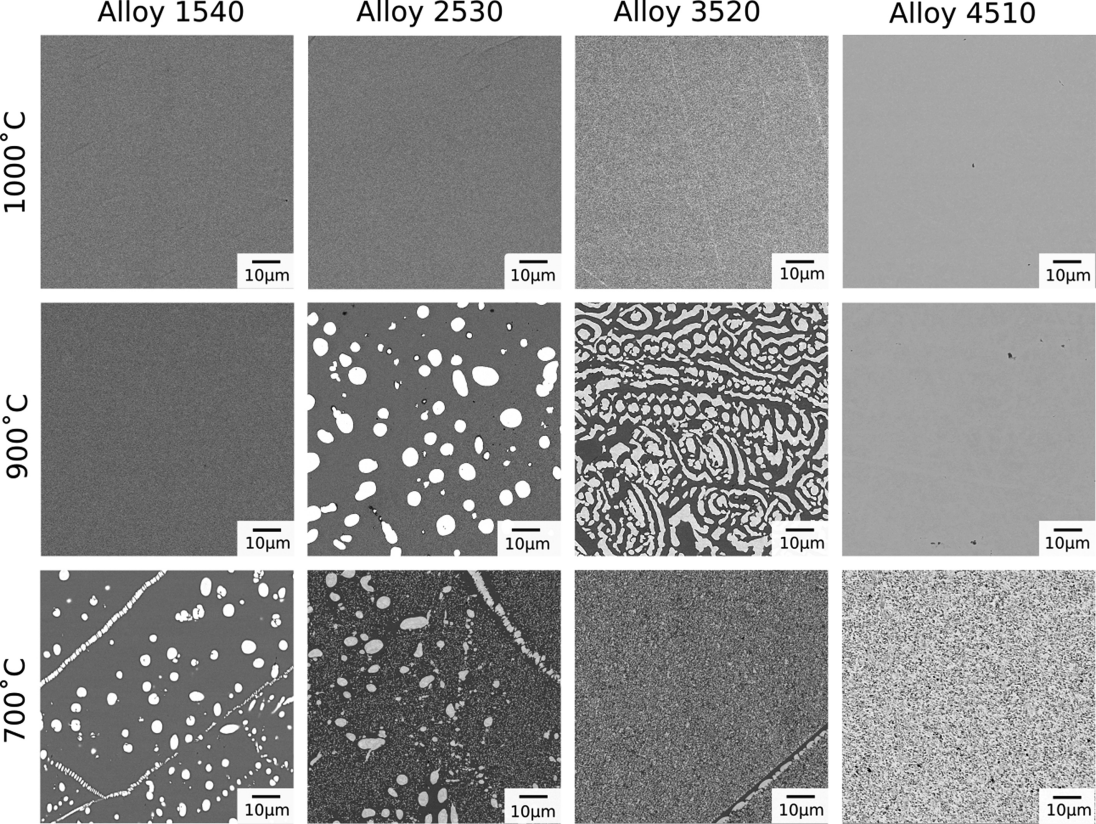
Alloy 1540
Alloy 2530
Alloy 3520
Alloy 4510
1000˚C
900˚C
700˚C
10μm

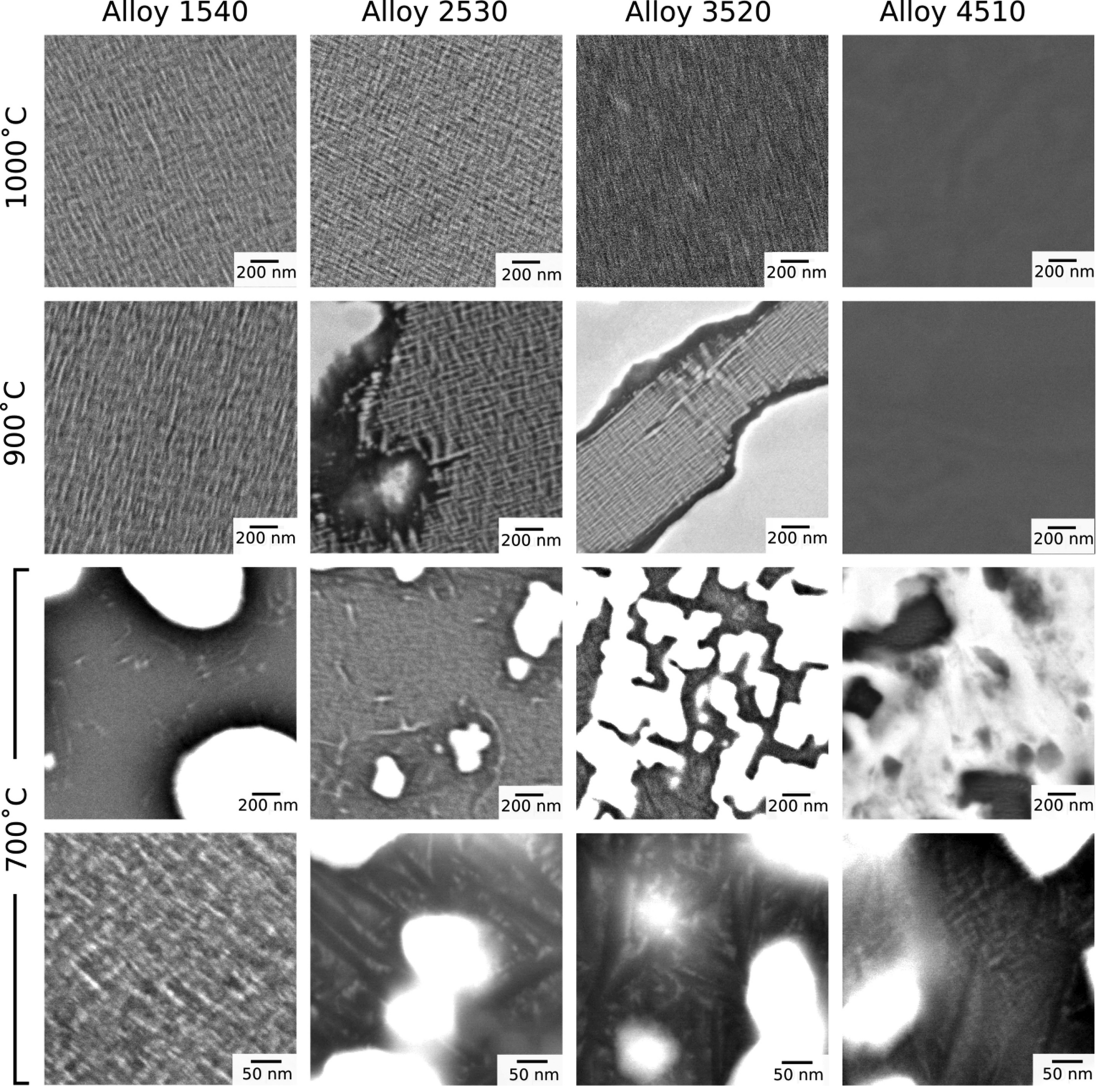
Alloy 1540
Alloy 2530
Alloy 3520
Alloy 4510
1000˚C
900˚C
700˚C
200 nm
50 nm

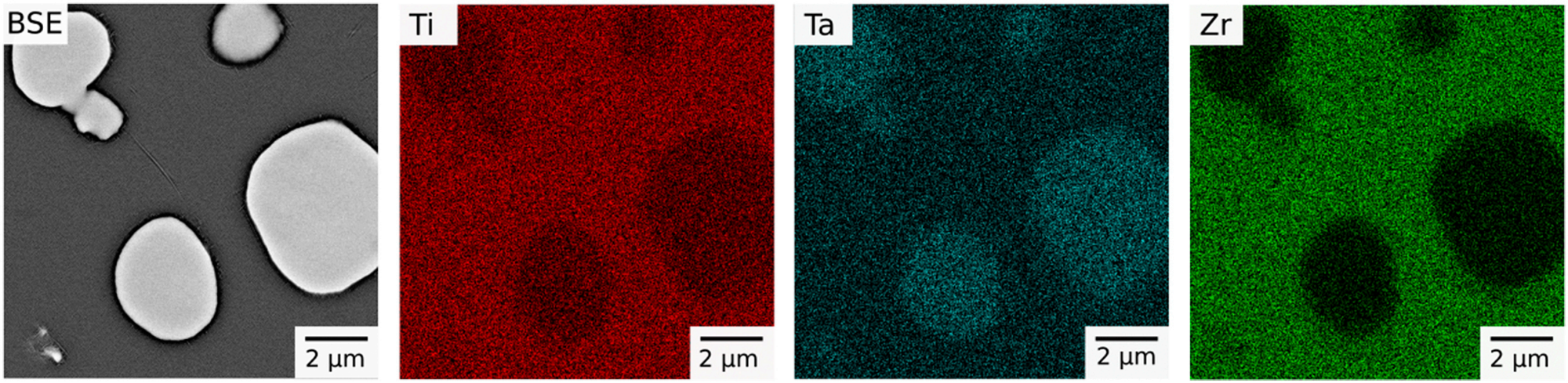
BSE
2 µm
Ti
2 µm
Ta
2 µm
Zr
2 µm

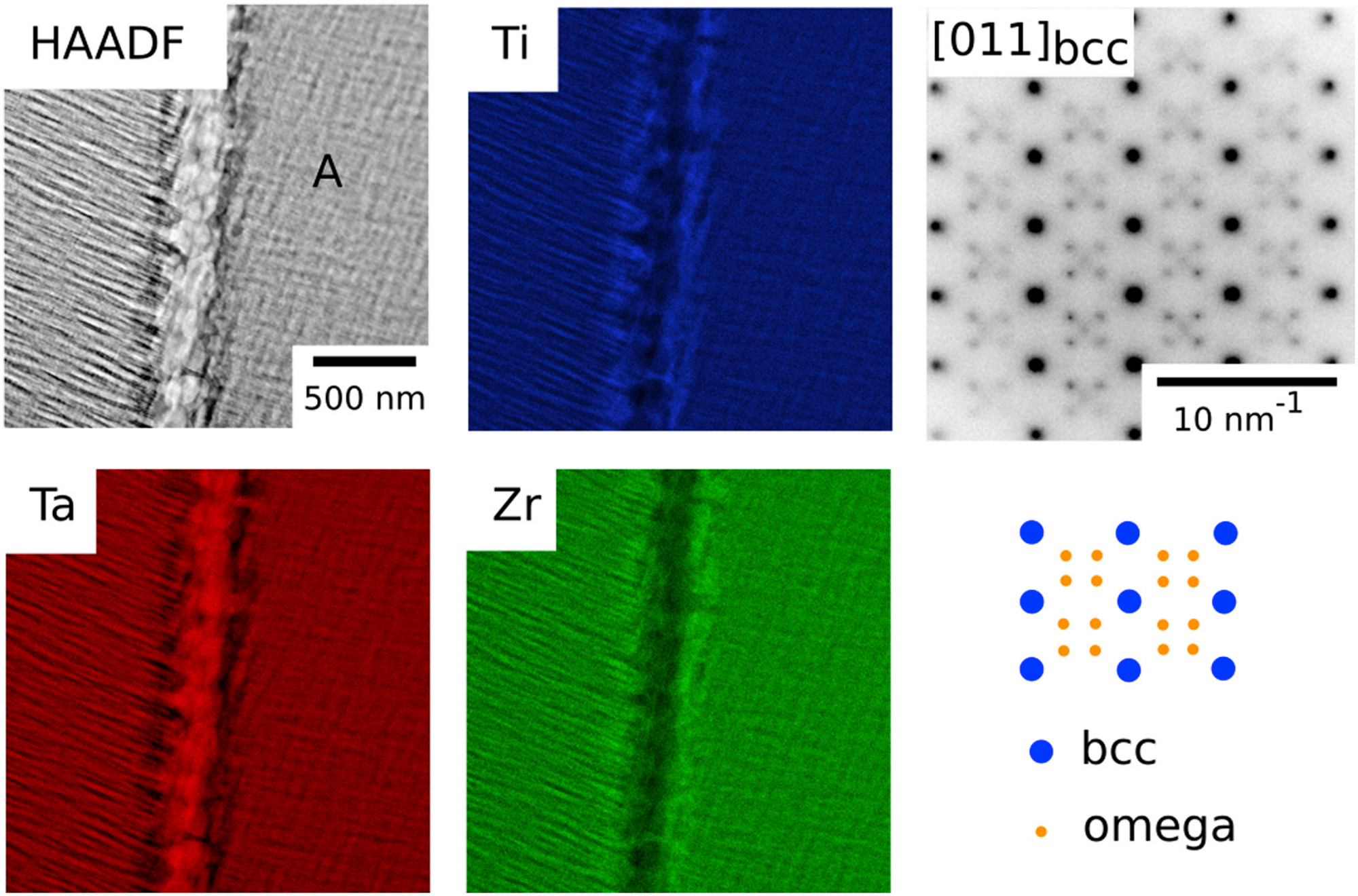
HAADF
A
500 nm
Ti
[011]bcc
10 nm-1
Ta
Zr
bcc
omega

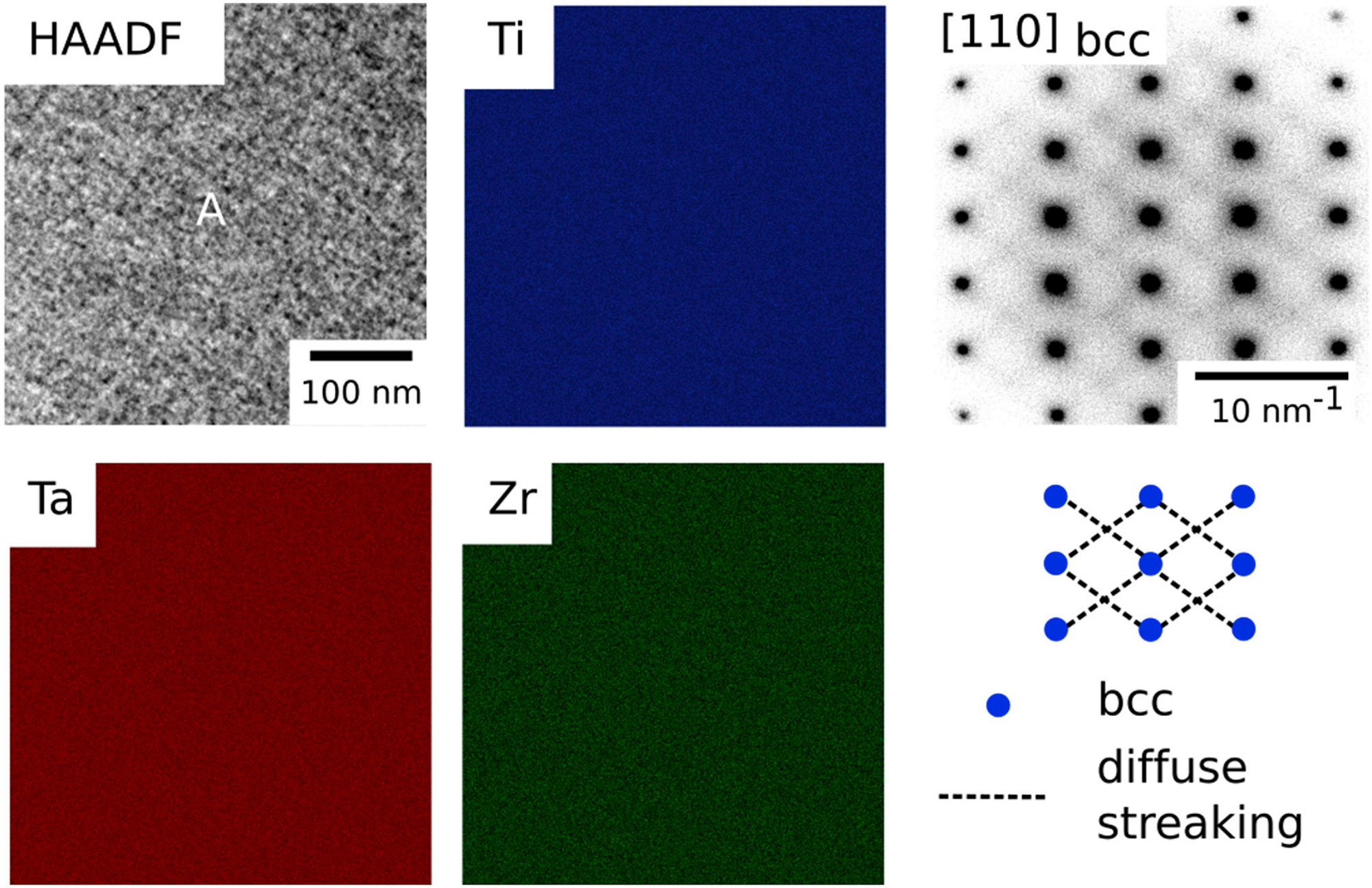
HAADF
A
100 nm
Ti
[110] bcc
10 nm-1
Ta
Zr
bcc
diffuse
streaking

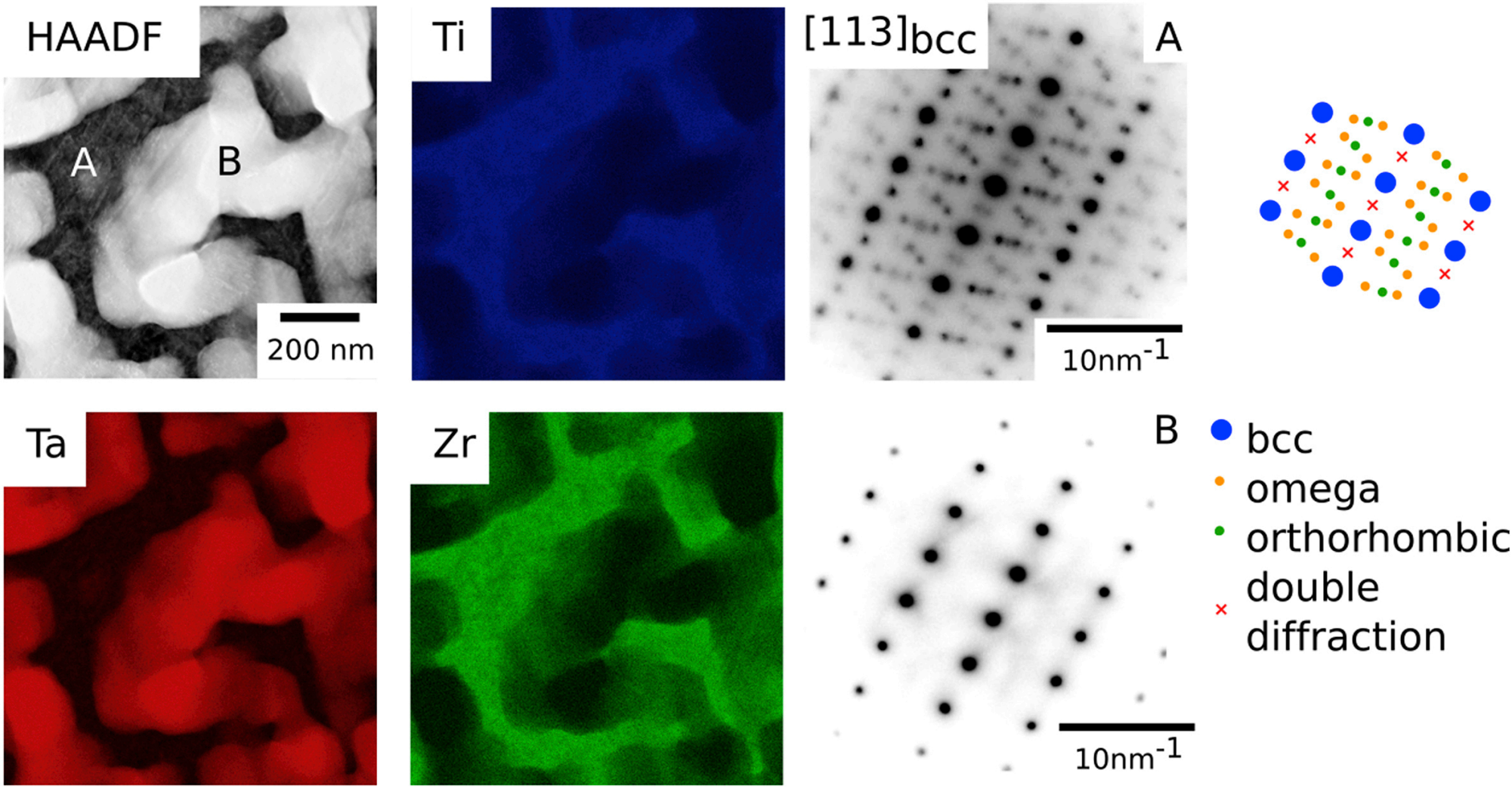
HAADF
A
B
200 nm
Ti
[113]bcc
A
10nm-1
Ta
Zr
B
10nm-1
bcc
omega
orthorhombic
double
diffraction

Highlights

Phase equilibria of Ti-Ta-Zr alloys studied as proxy to RM high entropy superalloys

Nanoscale phase morphology similar to RMHES produced in simplified Ti-Ta-Zr system

Single bcc phase at high temperatures; two bcc phases at intermediate temperatures

Nanostructures formed by spinodal decomposition due to Zr and Ta miscibility gap

Refractory metal matrix phase can be achieved by compositional variations

Declaration of Interest

Declarations of interest: none